TiO_2 Electrodes

International Edition: DOI: 10.1002/anie.201506357
German Edition: DOI: 10.1002/ange.201506357

TiO_2 Microboxes with Controlled Internal Porosity for High-Performance Lithium Storage

Xuehui Gao, Gaoran Li, Yangyang Xu, Zhanglian Hong, Chengdu Liang, and Zhan Lin**

Abstract: *Titanium dioxide (TiO_2) is considered a promising anode material for high-power lithium ion batteries (LIBs) because of its low cost, high thermal/chemical stability, and good safety performance without solid electrolyte interface formation. However, the poor electronic conductivity and low lithium ion diffusivity of TiO_2 result in poor cyclability and lithium ion depletion at high current rates, which hinder them from practical applications. Herein we demonstrate that hierarchically structured TiO_2 microboxes with controlled internal porosity can address the aforementioned problems for high-power, long-life LIB anodes. A self-templating method for the synthesis of mesoporous microboxes was developed through Na_2EDTA-assisted ion exchange of $CaTiO_3$ microcubes. The resulting TiO_2 nanorods were organized into microboxes that resemble the microcube precursors. This nanostructured TiO_2 material has superior lithium storage properties with a capacity of 187 mAh g^{-1} after 300 cycles at 1 C and good rate capabilities up to 20 C.*

Owing to its unique advantages of low cost, nontoxicity, small volume expansion (<4%), and high thermal and chemical stability, titanium dioxide (TiO_2) has attracted great interest as an attractive substitute of the conventional graphite anode for high-power lithium ion batteries (LIBs).[1] Furthermore, a stable solid electrolyte interface layer is not required at the relatively high TiO_2 working voltage (about 1.5 V vs. Li/Li^+), enabling TiO_2 to meet safety requirements of LIB anodes for electric vehicles.[2] However, such a high working voltage of anode reduces the working voltage of full cells, thus compromising the energy density of practical batteries. One of the solutions of high energy density is the use of thick electrodes. Rapid mass transport is crucial to high power batteries, particularly for using thick electrodes.[3] To achieve the rapid mass transport of lithium ions, nanostructuring of TiO_2 is widely sought to improve Li^+ diffusion at the active material level. Nevertheless, the close packing of nanomaterials leaves very limited porosity at the electrode level to allow rapid mass transport through the interior of the electrode to the electrolyte.[4] Therefore, high rate cycling of high energy batteries will always struggle with a limited mass transport rate between the electrode and electrolyte. A phenomenon of lithium ion depletion occurs at the internal porosity of practical electrodes.[5]

To alleviate mass transport at the electrode level, a few approaches have been reported to control the porosity and tortuosity of the electrode. For example, Chiang and coworkers used a co-extrusion method to produce porous electrodes by the sacrificial use of organic templates.[6] However, only limited success has been achieved on the control of electrode porosity because of the nature of forming dense structures of random particles. Herein, we manipulate the formation of electrode porosity through the morphologic engineering of active materials. This bottom-up approach allows the control of porosity of individual particles of active materials. The electrode porosity is thus predefined by the porosity and structure of the active material, instead of pore formation through conventional methods which are defined by the slurry coating process of the electrode after preparation treatments. Hollow microboxes of TiO_2 have been designed and synthesized to demonstrate the concept of preformed internal porosity of active materials.

Hollow micro/nano-structures with high surface area, large nanoscale interiors, and good mass permeability exactly meet the need of controlling the interior porosity of high-energy electrodes.[7] Various synthesis methodologies are well established for mesoporous hollow structures, including the Ostwald ripening method,[8] galvanic replacement,[9] and templating.[10] Generally, these methods require high temperatures, special conditions, and/or template removal.[11] All these synthesis and processing conditions increase costs and have limited capability for mass production. A template-free synthesis approach of nanostructured active material is highly desirable for practical applications. Herein, we first report a straightforward, effective route for the synthesis of hollow TiO_2 microboxes through a Na_2EDTA-assisted ion exchange (Figure 1). $CaTiO_3$ was first grown into microcubes with good uniformity using a solvothermal method, and they served as self-sacrificial templates for TiO_2 microboxes.[12] Then an ion exchange reaction occurred with the assistance of Na_2EDTA. The initial ion exchange generated a thin H_2TiO_3 layer on the surface of the $CaTiO_3$, which quickly transformed into TiO_2-

[*] X. H. Gao, G. R. Li, Y. Y. Xu, Prof. Z. Lin
Key Laboratory of Biomass Chemical Engineering of Ministry of Education
College of Chemical and Biological Engineering
Zhejiang University
Hangzhou 310027 (P.R. China)
E-mail: zhanlin@zju.edu.cn
X. H. Gao, Prof. Z. L. Hong
State Key Laboratory of Silicon Materials
School of Materials Science and Engineering
Zhejiang University
Hangzhou 310027 (P.R. China)
Dr. C. D. Liang
Center for Nanophase Materials Sciences
Oak Ridge National Laboratory
Oak Ridge, TN 37831 (USA)
E-mail: liangcn@ornl.gov

Supporting information for this article is available on the WWW under http://dx.doi.org/10.1002/anie.201506357.

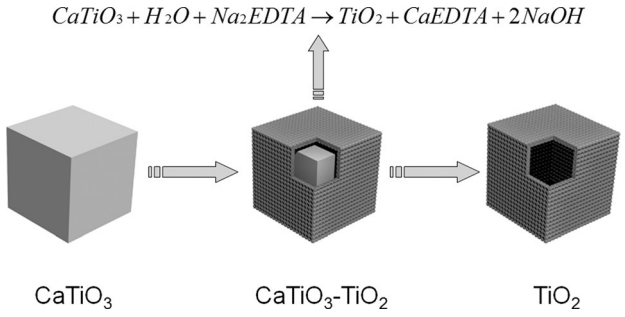

Figure 1. Schematic of the formation of hollow TiO_2 microboxes.

coated $CaTiO_3$ intermediates. A subsequent ion exchange between $CaTiO_3$ and H^+ ions led to the formation of hollow structures with mesoporous shells. The outward diffusion rate of Ca^{2+} ions is much faster than the inward diffusion rate of H^+ ions, which leads to the evacuation of Ca^{2+} in the inner region, generating a hollow interior.[13] The whole reaction is described in Equation (1):

$$CaTiO_3 + H_2O + Na_2EDTA \rightarrow TiO_2 + CaEDTA + 2\,NaOH \quad (1)$$

As a result, mesoporous TiO_2 microboxes were successfully obtained, although the conversion of complex metal oxides into simple metal oxides was reported before.[14] The detailed procedure is provided in the Supporting Information. Benefiting from unique structural features, the mesoporous TiO_2 microboxes exhibit superior lithium storage properties with a stable cycling capacity at 187 $mAh\,g^{-1}$ over 300 cycles at 1 C and enhanced rate capabilities up to 20 C, which is among the best cycling performances of TiO_2 anodes for LIBs to date.

Uniform $CaTiO_3$ microcubes were synthesized as self-sacrificial templates using a facile solvothermal method (Supporting Information). The morphological and crystallographic structures of the $CaTiO_3$ microcubes are shown in Figure 2. The X-ray diffraction (XRD) of $CaTiO_3$ microcubes (Figure 2 a) was indexed to its orthorhombic pattern (JCPDS card No. 22-0153) with no impurity peaks detected. The morphology of the phase-pure $CaTiO_3$ microcubes was characterized by field-emission scanning electron microscopy (FESEM) and transmission electron microscopy (TEM; Figure 2 b–d). A panoramic FESEM image shows the high uniformity of these $CaTiO_3$ microcubes with an average length of 0.9 μm (Figure 2 b). With high uniformity and relatively large size, the $CaTiO_3$ microcubes serve as templates for the formation of hollow TiO_2 microboxes through the Na_2EDTA-assisted ion-exchange route.The FESEM image at higher magnification further reveals the microcubic structure of $CaTiO_3$ with a smooth surface (Figure 2 c), and the TEM image confirms its solid texture (Figure 2 d).

Using the $CaTiO_3$ microcubes as self-sacrificial templates, we synthesized hollow TiO_2 microboxes with mesoporous shells through a Na_2EDTA-assisted ion exchange procedure under hydrothermal conditions (Figure 1). In the absence of Na_2EDTA during the reaction, the resulting product was only $CaTiO_3$ (Supporting Information, Figure S1), which indicates the important role of Na_2EDTA in the formation of TiO_2

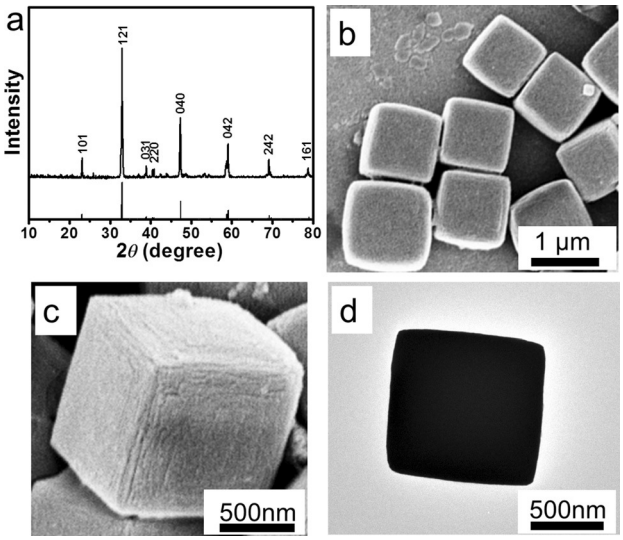

Figure 2. a) XRD pattern, (b, c) FESEM, and d) TEM images of $CaTiO_3$ microcubes.

hollow microboxes. Note that the use of a mixed solvent of ethylene glycol (EG) and deionized (DI) water is critical for the formation of uniform TiO_2 hollow microboxes. When the synthesis was carried out in an aqueous solution, a mixture of TiO_2 and $CaTiO_3$ was obtained (Supporting Information, Figure S2). When the synthesis was carried out in an EG solution, the only product was $CaTiO_3$ (Supporting Information, Figure S3). The formation of the mesoporous TiO_2 hollow microboxes was observed only in mixed solvents of EG and DI water. EG combines with more OH^- and, as a result, abundant H^+ participates in ion exchange with Ca^{2+} in $CaTiO_3$ and facilitates the formation of TiO_2. The relatively high viscosity of EG effectively slows down the reactivity and diffusion rate of reagents and favors structural integrity during the reaction.[15]

The high crystallinity and phase purity of the resulting material were confirmed by XRD (Supporting Information, Figure S4), which was indexed to anatase TiO_2 (JCPDS card No. 21-1272). TiO_2 microboxes, uniformly about 0.9 μm in size, were constructed by the roughly 0.1 μm shells of self-assembled nanorods (Figure 3 a,b). Their hollow interiors and detailed geometrical structure were further elucidated by TEM (Figure 3 c,d), which shows that they duplicated well the size and shape of $CaTiO_3$ precursor microcubes. The solid $CaTiO_3$ microcubes were fully converted into porous TiO_2 hollow structures, in good agreement with the SEM observation. Figure 3 e shows a high-resolution TEM image of the microboxes, in which an interplanar spacing of 0.35 nm is assigned to the (101) lattice plane of anatase TiO_2. The selected area diffraction pattern for TiO_2 hollow microboxes (Figure 3 f) indicates their high level of crystallinity, and each diffraction ring is also well indexed to anatase TiO_2. The chemical compositions were confirmed by energy-dispersive x-ray spectroscopy (EDX) analysis (Figure 3 g), which shows only pure Ti and O signals. The self-assembled TiO_2 nanorods formed mesoporous structures, as confirmed by N_2 adsorption/desorption isotherm analysis (Supporting Information,

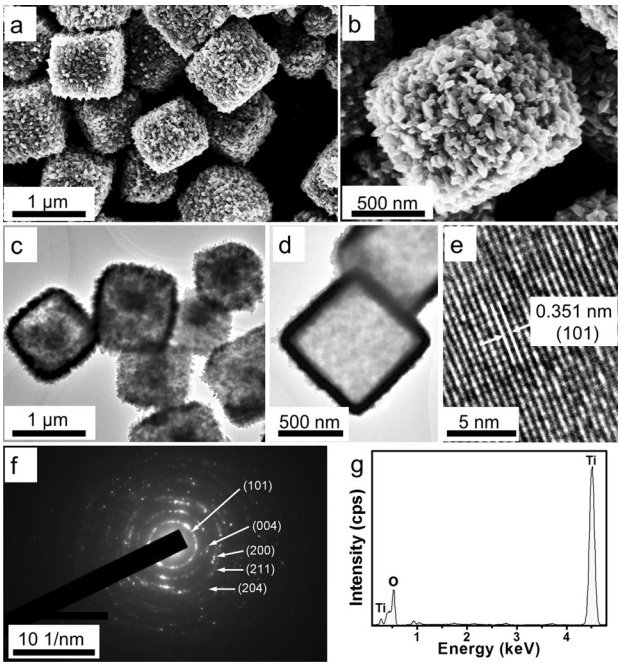

Figure 3. (a, b) FESEM and (c–e) TEM images of hollow TiO_2 microboxes (ca. 0.1 μm shell) with f) corresponding SAED pattern, and g) EDX analysis.

Figure S5). A Brunauer–Emmett–Teller (BET)-specific surface area of 30.3 $m^2 g^{-1}$ was obtained and the sizes of the mesopores were centered around 4 nm (Supporting Information, Figure S5, inset). Such a value of surface area is high for TiO_2 considering its relatively high bulk density of 3.78 $g cm^{-3}$. The microboxes contain two types of porosities: the mesopores that can be measured by the BET theory, and the macropores as the hollow interior, which can be estimated through the wall thickness and the size of the microboxes.

The importance of the internal porosity for high rate LIBs with practical loading is illustrated as follows by comparing the porosities of spheres, hollow spheres, cubes, and hollow microboxes, respectively. In Figure 3a and 3b, the size of the TiO_2 microboxes is uniformly about 0.9 μm with the 0.1 μm shells of self-assembled nanorods. The porosity of the microboxes is calculated as roughly 47.1 %. As a comparison, the closest theoretical packing of the cubes is zero in the porosity. For spherical particles, the porosity of the cubic closest packing (CCP) is approximately 25.9 %.[16] We assume that the hollow sphere is also 0.9 μm in the diameter with the 0.1 μm shell for comparison. The calculated porosity of the hollow spheres is 47.1 %. When taking the theoretical porosity of the whole electrode into consideration, the porosities for the spheres, hollow spheres, cubes, and hollow microboxes are 25.9 %, 73.0 %, 0 %, and 47.1 %, respectively. When taking both the energy density and power density into consideration, a porosity of 50 % of cell volume is required for high energy density of LIBs.[6] Given the 47.1 % porosity from the hollow core and 1 % additional porosity from the mesoporous wall, the total porosity is approximately 48.1 % for hollow TiO_2 microboxes. This means that the design of the hollow microboxes matches well with the requirements for optimum porosity of high power and high energy LIBs. Moreover, the structures of TiO_2 microboxes can be designed for different sizes and porosities to meet the requirements of real LIB anodes for practical applications.[12] It is anticipated that the mesoporous channels on the wall of the microboxes will improve Li-ion diffusion and ensure intimate contact between the active material and the electrolyte for high-rate of mass transport at the TiO_2 anodes in LIBs.

TiO_2 hollow microboxes were evaluated as anode materials for lithium storage properties in LIBs. The electrochemical lithium insertion properties of the microboxes were investigated in a Li/TiO_2 half-cell configuration by cyclic voltammetry (CV) between 1 and 3 V at a slow scan rate of 0.1 $mV s^{-1}$ (Figure 4a). The cathodic/anodic peaks located at

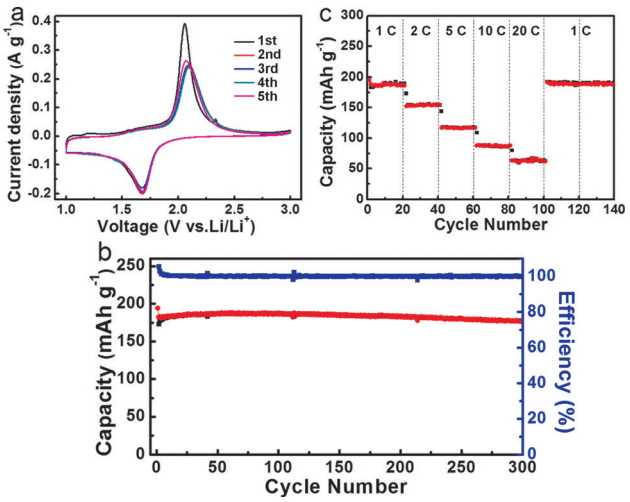

Figure 4. a) CV curves of hollow TiO_2 microboxes between 3 and 1 V with a scan rate of 0.1 $mV s^{-1}$. b) Cycling performance of hollow TiO_2 microboxes at a current density of 1 C with corresponding coulombic efficiency. c) Rate performance of anatase TiO_2 microboxes at various current rates from 1 to 20 C.

1.68 and 2.06 V (vs. Li/Li^+) are associated with lithium insertion and extraction, respectively, in the anatase lattice, which is consistent with previously reported data. No obvious change in cathodic peak potential was observed after the first cycle, demonstrating the good reversibility of the structures in electrochemical reactions. The galvanostatic charge-discharge profiles of the TiO_2 microbox electrode with different cycles (for example, cycle number 1, 2, 10, 100, and 300) were demonstrated (Supporting Information, Figure S6). These profiles exhibit two voltage plateaus at 1.75 V for lithium insertion and 2.0 V for lithium extraction, respectively, which are consistent with the CV curves. Figure 4b shows the cycling performance and the coulombic efficiency of TiO_2 hollow microboxes at a current density of 1 C (1 C = 170 $mA g^{-1}$). The initial discharge capacity was 205 $mAh g^{-1}$, indicating a coulombic efficiency of 89.1 %. The discharge capacity then decayed to 193 $mAh g^{-1}$ in the first 10 cycles and remained very stable up to 300 cycles at 187 $mAh g^{-1}$. The coulombic efficiency remained nearly 100 % after the first few cycles, which demonstrate the high reversibility of TiO_2 hollow

microboxes for lithium storage during cycling. The FESEM images of the TiO_2 microbox electrode after 300 cycles show there are no obvious morphological changes in the electrode, although there are some inevitable minor structural defects in microboxes during cycling (Supporting Information, Figure S7). As a result, the stability in the microbox structure and the integrity in the electrode are responsible for the stable performance for lithium storage in long-term cycling. TiO_2 microbox electrodes were also investigated for rate capability (Figure 4c). They showed high capacities at different current rates; even at a very high current rate of 20 C (3400 $mA\,g^{-1}$), a reversible capacity of 63 $mAh\,g^{-1}$ was still delivered. When the current was cycled back to 1 C, a capacity of 190 $mAh\,g^{-1}$ was resumed, indicating outstanding high-rate cycling performance resulting from their good structural stability. The cycling stability of TiO_2 microbox electrodes at high current rates of 10 and 20 C was also shown (Supporting Information, Figure S8). There were almost no obvious discharge capacity decays up to 1000 cycles, which further confirm excellent structural stability of TiO_2 microboxes for long-term cycling even at high rate capabilities. The high cycling stability of TiO_2 hollow microboxes is superior to that of other anatase TiO_2 micro/nanostructures, and the high rate performance is among the best demonstrated (Supporting Information, Table S1). These findings indicate TiO_2 hollow microboxes are capable of stable electrochemical cycling with high power density.

Clearly, the outstanding electrochemical performance of TiO_2 electrodes originates from the porosity control through hollow structure and the advantages of microbox structures. The hollow microboxes are composed of small nanorods, between which finite mesoporous shells enable easy diffusion of Li^+ ions by shortening transport length. The high surface area provides more active sites and a large electrolyte-electrode contact area for Li^+ insertion and surface Li storage. The robust, micro-size shell structure effectively prevents the undesirable aggregation of conventional nanoparticles, which ensures the integrity of the electrode and improves capacity retention upon prolonged cycling. Finally, the large porosity in the hollow structure provides enough space to accommodate a liquid electrolyte, which supplies the necessary Li^+ ions during cycling at high current rates to avoid Li^+ depletion. These features ensure TiO_2 anodes with high specific capacity, a long cycle life, and promote fast, reversible Li insertion and extraction at high current rates.

To confirm the importance of controlled internal porosity for high-performance lithium storage, we intentionally designed TiO_2 microboxes with different internal porosities. As discussed above, we synthesized TiO_2 microboxes with 0.1 μm shells and the internal porosity was calculated as 47.1 %, when volume ratio of EG to DI water is 1:3. The internal porosity of TiO_2 microboxes can be controlled by varying the volume proportion of EG and DI water. When the volume ratio of EG to DI water was changed to 3:5, TiO_2 microboxes with shells of 0.15 μm (Supporting Informatino, Figure S9) and porosity of 29.6 % were also obtained. We further reduced internal porosity of TiO_2 microboxes by destroying their hollow microbox structures with high-energy ball-mill. The above two samples were denoted as TiO_2 microboxes (0.15 μm shell) and TiO_2 microboxes (crashed), respectively, which were utilized for comparisons in cycling performance (Supporting Information, Figure S10). TiO_2 microboxes (0.15 μm shell) and TiO_2 microboxes (crashed) delivered discharge capacity of 166 and 116 $mAh\,g^{-1}$ after 100 cycles, respectively, which is much lower than that of TiO_2 microboxes with 0.1 μm shell (197 $mAh\,g^{-1}$). Their rate capabilities were also much poorer than that of TiO_2 microboxes with 0.1 μm shell (Supporting Information, Figure S11). It is worth noting that not only the lower internal porosity but also structural instability are responsible for the worse cycling performance of TiO_2 microboxes (crashed).

In summary, we demonstrated the concept of predefined internal porosity through morphological engineering of each individual particle of TiO_2 as high performance anode materials for LIBs. Comparing with previous micro/nanostructured metal oxides (Supporting Information, Table S2), the synthesis of hollow TiO_2 microbox materials by self-sacrificial templates offers practical value for low-cost mass production of electrode materials. A hierarchically porous structure of TiO_2 microboxes with controlled internal porosity meets the optimum porosity of LIB electrodes with high power and high energy. The hollow TiO_2 microbox anodes showed significant improvement of lithium storage, compared with other TiO_2 meso/microporous structures, with stable cycling capacity at 187 $mAh\,g^{-1}$ over 300 cycles at 1 C and enhanced rate capability up to 20 C. This concept presents the battery field a new approach for the fine tuning of electrode internal porosity. The uniform hollow structures might be model systems for basic research of the mass transport phenomenon in porous electrodes and a broad scope of applications in which mass transport is a key parameter, for examples, catalysis, sensor, and separation.[17]

Acknowledgements

Z. Lin thanks the funding support from Chinese government under the "Thousand Youth Talents Program". C. Liang's effort was sponsored by the Division of Materials sciences and engineering, Office of Basic Energy Sciences U.S. Department of Energy (DOE). A portion of the electrochemical analysis was conducted at the Center for Nanophase Materials Sciences, which is a DOE Office of Science User Facility.

Keywords: battery · hydrothermal · lithium ion · microbox · TiO_2

How to cite: *Angew. Chem. Int. Ed.* **2015**, *54*, 14331–14335
Angew. Chem. **2015**, *127*, 14539–14543

[1] a) M. Wagemaker, A. P. M. Kentgens, F. M. Mulder, *Nature* **2002**, *418*, 397; b) H. Han, T. Song, J. Y. Bae, L. F. Nazar, H. Kim, U. Paik, *Energy Environ. Sci.* **2011**, *4*, 4532; c) S. W. Kim, T. H. Han, J. S. Kim, H. Gwon, H. S. Moon, S. W. Kang, S. O. Kim, K. Kang, *ACS Nano* **2009**, *3*, 1085; d) L. W. Ji, Z. Lin, M. Alcoutlabi, X. Zhang, *Energy Environ. Sci.* **2011**, *4*, 2682.

[2] a) H. Ren, R. B. Yu, J. Y. Wang, Q. Jin, M. Yang, D. Mao, D. Kisailus, H. J. Zhao, D. Wang, *Nano Lett.* **2014**, *14*, 6679; b) H. G. Jung, N. Venugopal, B. Scrosati, Y. K. Sun, *J. Power Sources* **2013**, *221*, 266.

[3] J. Choi, S. Lee, J. Ha, T. Song, U. Paik, *Nanoscale* **2013**, *5*, 3230.
[4] H. Buqa, D. Goers, M. Holzapfel, M. E. Spahr, P. Novak, *J. Electrochem. Soc.* **2005**, *152*, A474.
[5] a) P. A. Johns, M. R. Roberts, Y. Wakizaka, J. H. Sanders, J. R. Owen, *Electrochem. Commun.* **2009**, *11*, 2089; b) C. L. Li, X. X. Guo, L. Gu, D. Samuelis, J. Maier, *Adv. Funct. Mater.* **2011**, *21*, 2901.
[6] C. J. Bae, C. K. Erdonmez, J. W. Halloran, Y. M. Chiang, *Adv. Mater.* **2013**, *25*, 1254.
[7] a) X. H. Gao, H. B. Wu, L. X. Zheng, Y. J. Zhong, Y. Hu, X. W. Lou, *Angew. Chem. Int. Ed.* **2014**, *53*, 5917; *Angew. Chem.* **2014**, *126*, 6027; b) J. Luo, X. Xia, Y. Luo, C. Guan, J. Liu, X. Qi, C. F. Ng, T. Yu, H. Zhang, H. J. Fan, *Adv. Energy Mater.* **2013**, *3*, 737; c) J. H. Pan, X. Zhang, A. J. Du, D. D. Sun, J. O. Leckie, *J. Am. Chem. Soc.* **2008**, *130*, 11256.
[8] a) X. W. Lou, Y. Wang, C. Yuan, J. Y. Lee, L. A. Archer, *Adv. Mater.* **2006**, *18*, 2325; b) J. Li, H. C. Zeng, *J. Am. Chem. Soc.* **2007**, *129*, 15839.
[9] a) S. E. Skrabalak, L. Au, X. D. Li, Y. N. Xia, *Nat. Protoc.* **2007**, *2*, 2182; b) Y. Sun, B. Mayers, Y. N. Xia, *Adv. Mater.* **2003**, *15*, 641.
[10] a) D. Chen, J. Ye, *Adv. Funct. Mater.* **2008**, *18*, 1922; b) G. Q. Zhang, H. B. Wu, T. Song, U. Paik, X. W. Lou, *Angew. Chem. Int. Ed.* **2014**, *53*, 12590; *Angew. Chem.* **2014**, *126*, 12798.
[11] a) L. Zhang, H. B. Wu, B. Liu, X. W. Lou, *Energy Environ. Sci.* **2014**, *7*, 1013; b) L. Zhang, H. B. Wu, Y. Yan, X. Wang, X. W. Lou, *Energy Environ. Sci.* **2014**, *7*, 3302.
[12] a) X. Yang, I. D. Williams, J. Chen, J. Wang, H. Xu, H. Konishi, Y. Pan, C. Liang, M. Wu, *J. Mater. Chem.* **2008**, *18*, 3543; b) X. Yang, J. Fu, C. Jin, J. Chen, C. Liang, M. Wu, W. Zhou, *J. Am. Chem. Soc.* **2010**, *132*, 14279; c) Q. L. Wu, X. F. Yang, W. Z. Zhou, Q. Gao, F. Q. Lu, J. L. Zhuang, X. F. Xu, M. M. Wu, H. J. Fan, *Adv. Mater. Interfaces* **2015**, DOI: 10.1002/admi.201500210.
[13] a) W. L. Yang, L. Zhang, Y. Hu, Y. J. Zhong, H. B. Wu, X. W. Lou, *Angew. Chem. Int. Ed.* **2012**, *51*, 11501; *Angew. Chem.* **2012**, *124*, 11669; b) W. L. Yang, Y. Liu, Y. Hu, M. J. Zhou, H. S. Qian, *J. Mater. Chem.* **2012**, *22*, 13895; c) J. J. Li, W. L. Yang, J. Q. Ning, Y. J. Zhong, Y. Hu, *Nanoscale* **2014**, *6*, 5612.
[14] J. Park, H. Zheng, Y. W. Jun, A. P. Alivisatos, *J. Am. Chem. Soc.* **2009**, *131*, 13943.
[15] Z. Q. Li, X. S. Lin, L. Zhang, X. T. Chen, Z. L. Xue, *CrystEngComm* **2012**, *14*, 3495.
[16] http://En.Wikipedia.Org/Wiki/Close-Packing of Equal Spheres.
[17] a) J. F. Ye, W. Liu, J. G. Cai, S. Chen, X. W. Zhao, H. H. Zhou, L. M. Qi, *J. Am. Chem. Soc.* **2011**, *133*, 933; b) L. Xin, Y. Liu, B. J. Li, X. Zhou, H. Shen, W. X. Zhao, C. L. Liang, *Sci. Rep.* **2014**, *4*, 1; c) G. R. Li, M. Ling, Y. F. Ye, Z. P. Li, J. H. Guo, Y. F. Yao, J. F. Zhu, Z. Lin, S. Q. Zhang, *Adv. Energy Mater.* **2015**, DOI: 10.1002/aenm.201500878; d) H. Hu, L. Yu, X. H. Gao, Z. Lin, X. W. Lou, *Energy Environ. Sci.* **2015**, *8*, 1480.

Received: July 10, 2015
Revised: August 19, 2015
Published online: October 2, 2015

